Broadband High-Gain Beam-Scanning Antenna Array for Millimeter-Wave Applications

Chun-Xu Mao, Steven Gao, *Senior Member, IEEE*, and Yi Wang, *Senior Member, IEEE*

***Abstract*—In this paper, an integrated millimeter-wave filtering antenna array with low cost, broad bandwidth and high gain is proposed. The proposed 4 × 4 array serves as the unit subarray of a 2 × 2 multiple inputs multiple outputs (MIMO) antenna. The antenna element is designed based on a 3rd-order filter topology where the patch is treated as a resonator. To achieve a 3rd-order filtering characteristics, the patch is coupled with an U-shaped slot resonator in the ground plane and then a stub loaded resonator. The proposed vertically coupled structure not only makes the design very compact but also provides the strong coupling and therefore broaden the bandwidth of antenna. The seamless integration and co-design of the antenna and filter removes the need of a separate filter as required in traditional wireless systems. This potentially leads to significant reduction of the cost of RF front ends. To validate the concept, the subarray and the MIMO array at Ka band are optimized, prototyped and tested. Measured results agree well with the simulations, showing a broad bandwidth from 24.8 to 30.6 GHz, high in-band gain of 18 dBi and high cross polarization discrimination (XPD) of 30 dB. The presented antenna could have potential applications in 5G base-stations.**

***Index Terms*— Broadband, beam-switching, integration, filtering, antenna array, massive MIMO, 5G wireless communications.**

I. Introduction

The emerging fifth generation (5G) mobile communication has attracted intensive research interests in academia and industry because of its huge potentials such as broadband, very high data rate and significant reduction of digital traffic [1]-[2]. In the 5G era, lots of things such as electronic devices, vehicles and the equipment in the offices and homes will be wirelessly connected through Internet. Users will be able to access ultra-high-definition (UHD) multimedia streaming and services such as Virtual Reality (VR) and Augmented Reality (AR) [2]. It is widely believed the 5G standards will be introduced in 2020.

To meet the life-like experience of 5G users, one of the key demands for 5G communication is the extremely high data rate, which can be facilitated by increasing the bandwidths of the systems and operating in millimeter wave (mm-wave) frequency ranges. As the key transmitting/receiving components, the base-station antennas in mm-wave mobile broadband system are required to have high gain and adaptive directional beam so as to overcome the higher loss of the transmission path and improve the link stability [2]. Massive MIMO base station is another promising technique in improving the capacity and service quality by accurately concentrating the transmitted energy to the mobile users [3]-[5]. Fig. 1 shows the architecture of a massive MIMO antenna array for 5G base-station, consisting of multiple sub-arrays in two dimensions. The subarrays in the massive MIMO base station adaptively direct the beams to the users in azimuth and elevation directions. Each subarray is composed of $n \times n$ radiation elements and therefore high gain and steerable beam can be achieved. Due to the short wavelength of mm-waves and the limited coverage area of each 5G cellular, more base-stations will be required in urban areas. As a result, low-cost and light weight base station antennas will be in huge demand.

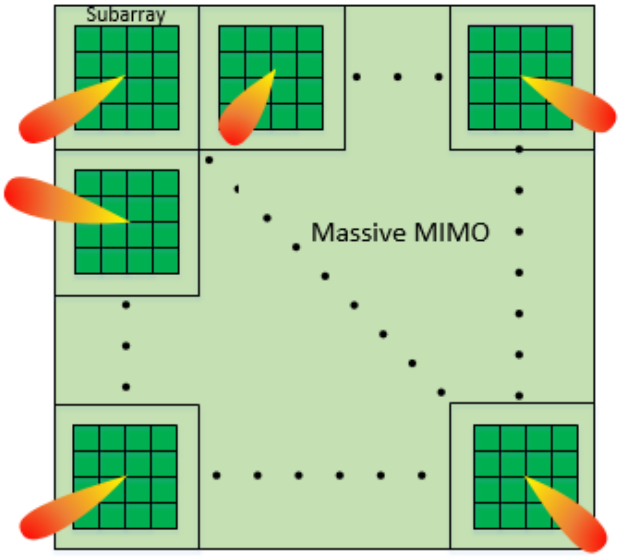

Fig. 1. Architecture of the massive MIMO antenna array for base-station.

Various mm-wave antenna elements have been reported for 5G communications [6]-[8]. In [6], a stacked patch antenna element was proposed to realize a broadband operation at 28 GHz. However, this antenna suffers from poor radiation

Manuscript submitted on April 30, 2016; This work is supported by the EPSRC grant EP/N032497/1 and YW is supported by UK EPSRC under Contract EP/M013529/1.

C. Mao and S. Gao are with School of Engineering and Digital Arts, University of Kent, Canterbury, UK (email: cm688@kent.ac.uk).

Y. Wang is with the Department of Engineering Science, University of Greenwich, UK (email: yi.wang@gre.ac.uk).

performance in E- and H-plane with some nulls in the main beam. In [7], a tilted antenna at 28 GHz was reported by combining a patch and a waveguide aperture. The design is compact, but difficult for integration because of the adopted waveguide. Dual-band (28/38 GHz) antenna elements with circular polarization have also been proposed in [8], but the antenna suffers from narrow bandwidths (less than 3%). Mm-wave antenna arrays for 5G applications were also demonstrated in [9]-[11]. In [9], a large-scale array at 28 GHz was achieved in a cell phone. Mm-wave arrays using substrate integrated waveguide (SIW) and low temperature co-fired ceramic (LTCC) technologies are also realized in [10]-[11]. In [12]-[14], massive MIMO arrays for 5G wireless communications were presented. In [12], a waveguide slot array at 60 GHz was proposed. Massive MIMO arrays based on using low-cost patch antennas were shown in [13] and [14], but their bandwidths were limited and the antenna subarrays were placed in different planes.

As mentioned earlier, in order to meet the requirements of 5G wireless applications, antenna arrays with broadband, low-profile and low-cost are required. Techniques such as massive MIMO and beam-switching need to be employed in the antenna design. In addition, the integration of passive components is another promising approach to further reduce the complexity and cost of the RF frontends [15]-[16]. For instance, integrated filtering antennas can not only reduce the interferences from other channels and losses but also enhance the bandwidth and frequency selectivity [17]. In this paper, a 2 × 2 massive MIMO array based on integrated filter-antenna is proposed. Each channel of the MIMO is a 4 × 4 subarray that delivers high gain. Besides, the beam-switching capability of the subarray is investigated. Vertically coupled resonators are used to achieve a very compact footprint but obtain a 3rd-order broadband filtering characteristic. The subarray and massive MIMO antenna array are prototyped and tested to verify the design concept.

This paper is organized as follows. Section II illustrates the subarray and design methodology. Section III covers the massive MIMO antenna array. Section IV presents the results followed by Conclusions.

II. Antenna Element and Subarray

A. Configuration of subarray

Fig. 1 shows the configuration of the proposed subarray, which is composed of 4 × 4 radiation elements. It has a stacked structure. The patches are printed on the top layer of the upper substrate while the feeding network is printed on the bottom layer of the lower substrate. Between the two substrates, a 1 mm thick foam is inserted as a spacer. The patches and the feeding network share the same ground plane, which is placed on the top layer of the lower substrate. In the ground plane, two U-shaped slots for every patch are etched to form a resonator and couple the electromagnetic wave from the feed to the patches. RO 4003C substrate with a permittivity of 3.55 and loss tangent of 0.0027 is used for the lower substrate while RO 5880 substrate with a permittivity of 2.2 and loss tangent of 0.0009 is used for the upper substrate. The thicknesses of the RO 4003C and the RO 5880 are 0.2 mm and 0.254 mm, respectively. In order to reduce the grating lobe level for the beam switching applications, the spacing between the elements *Ld* is chosen to be 0.6 λ at 28 GHz.

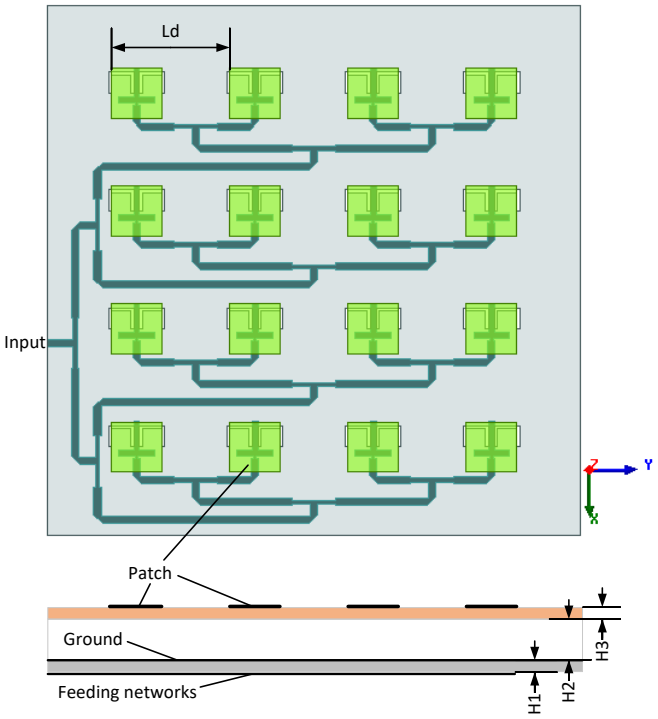

Fig. 1. Configuration of the proposed 4 × 4 subarray. *Ld* = 6.4 mm, *H1* = 0.2 mm, *H2* = 1 mm, *H3* = 0.254 mm.

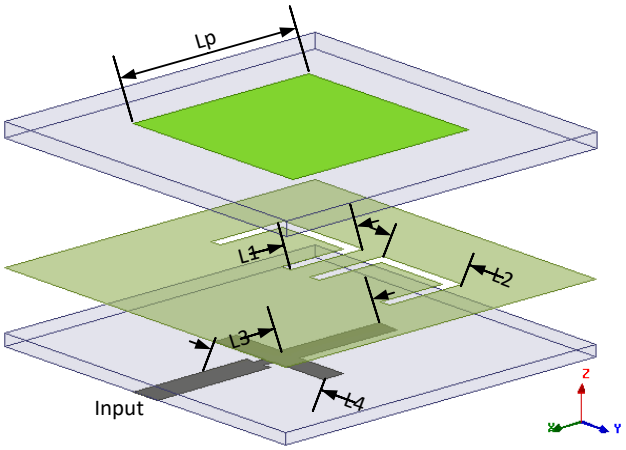

Fig. 2. Configuration of the antenna element. *Lp* = 3.2 mm, *L1* = 1.4 mm, *L2* = 1.6 mm, *L3* = 1.9 mm, *L4* = 2.1 mm.

B. Antenna element

The radiation element in the subarray is shown in Fig. 2. Different from a traditional patch antenna, two U-shaped slots are inserted in the ground. The slots works as half-wavelength resonators. Two slots instead of one are utilized here to balance the coupling to the patch and reduce the cross polarization level.

The slots resonators are symmetrical with respect to the feed line in the bottom layer. The feeding line is tapped to a symmetrical stub loaded resonator (SLR). Here, the SLR serves as a single mode resonator as only the even mode is excited. The patch, U-shaped slot resonator and SLR have the same resonant frequency of 28 GHz. The dimensions of the slots and the SLR can be approximately determined using the expressions below,

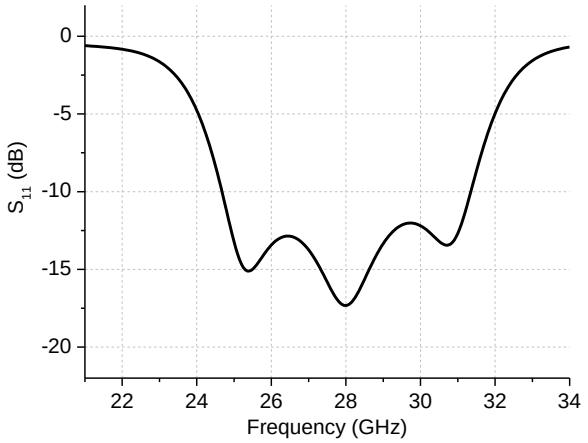

Fig. 3. Simulated S_{11} of the proposed antenna element.

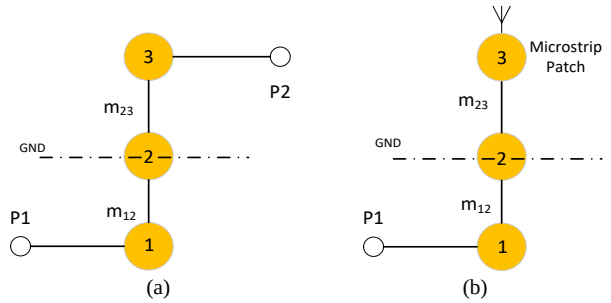

Fig. 4. Topologies of the coupled-resonator structures: (a) a bandpass filter; (b) the proposed integrated filtering antenna element in Fig. 2.

$$2L1 + L2 \approx \frac{c}{2 f_0 \sqrt{\varepsilon_{eff1}}} \quad (1)$$

$$L3 + \frac{L4}{2} \approx \frac{c}{2 f_0 \sqrt{\varepsilon_{eff2}}} \quad (2)$$

where f_0 is the resonant frequency. ε_{eff1} and ε_{eff2} are the effective dielectric constants of the slot-line in the ground and the microstrip, respectively. c is the speed of light in free space. The optimization was performed using high frequency structural simulator (HFSS 15) and the optimized parameters are presented in the legend of Fig. 2.

Since the patch, U-shaped slots and SLR are vertically coupled and synchronously tuned, the proposed antenna element has a compact size and exhibits a 3rd-order frequency response, as shown in Fig. 3. As can be observed, the antenna element has a broad impedance bandwidth from 24.5 to 31.5 GHz (FBW=25%) with three reflection zeros in the operation band. The filtering characteristic of the antenna is attributed to the integrated design, which will be discussed further in the next section.

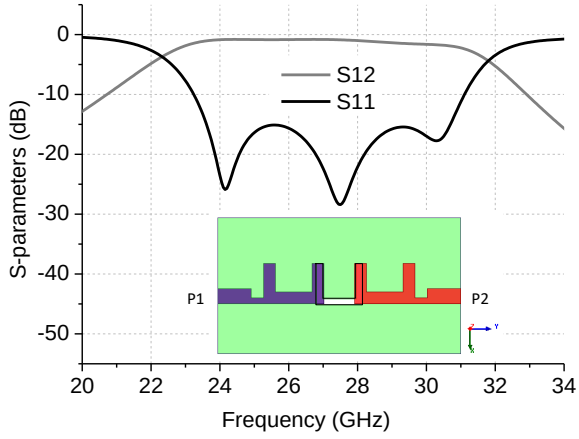

(a)

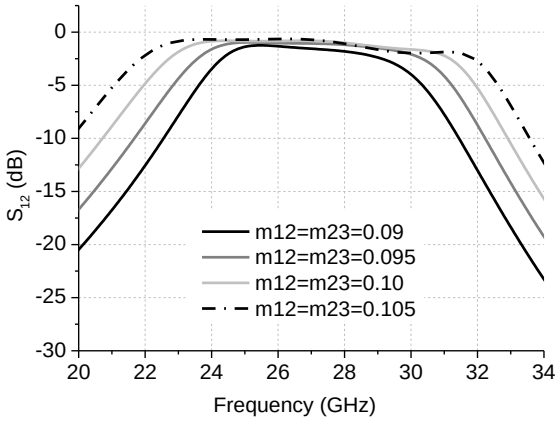

(b)

Fig. 5. (a) Simulated S-parameters of the bandpass filter; (b) bandwidth variation with different coupling coefficients.

III. Design Methodology

The coupled-resonator structure shown in Fig. 2 helps the antenna element to achieve a very wide bandwidth with a compact size. This integrated filtering antenna is realized using a coupled filter design approach, where the patch is treated as the last resonator of a 3rd-order filter.

A. Topology and vertically coupled bandpass filter

Fig. 4(a) shows the topologies of a vertically coupled 3rd-order bandpass filter. The circles represent the resonators whereas the lines represent the coupling between them. It is important to note that here the resonator-2 is a defected ground structure. Such a stacked configuration effectively reduces the footprint of the design. Replacing the 3rd resonator with a patch antenna leads to the 3rd-order filtering antenna, as shown in Fig. 4(b).

First, a bandpass filter is designed to demonstrate the broadband capability for the strong coupling between the vertically coupled resonators. As shown in Fig. 5(a), a very broadband from 23.2 to 30.8 GHz can be achieved using two microstrip hairpin resonators and one slot-line resonator in the

ground. By adjusting the coupling intensity between the resonators, the bandwidth of the filter can be changed, as presented in Fig. 5(b). This can also be applied to adjust the bandwidth of the proposed integrated filtering antenna.

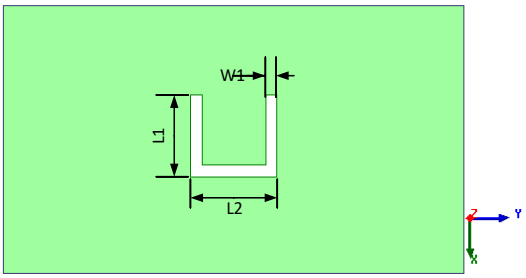

Fig. 6. Configuration of the U-shaped slot resonator.

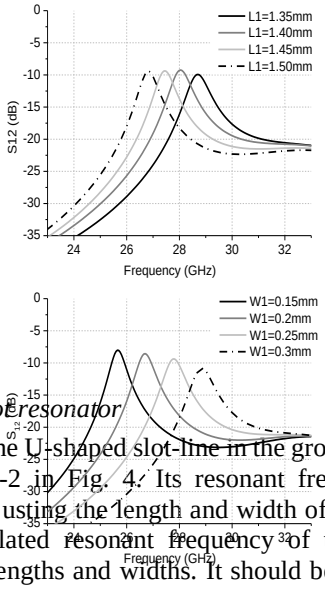

B. *U-shaped slot resonator*

Fig. 6 shows the U-shaped slot-line in the ground, which acts as the resonator-2 in Fig. 4. Its resonant frequency can be controlled by adjusting the length and width of the slot. Fig. 7 shows the simulated resonant frequency of the slot as the function of the lengths and widths. It should be noted that the width of the slot has a significant effect on the resonant frequency. In this design, *W1*=0.2 mm is chosen.

C. *Filter antenna integration*

To illustrate the filter-antenna integration scheme, three types of patch antennas are investigated, as shown in Fig. 8. Fig. 8(a) is a traditional slot coupled patch antenna fed by a microstrip at the center, denoted as Antenna-I. Replacing the slot in the ground by a half-wavelength U-shaped slot and feeding from one side, lead to Antenna-II in Fig. 8(b). Fig. 8(c) represents the proposed antenna in this work. Different from Antenna-II, there are two U-shaped slots side-by-side. The microstrip feed line is tapped to an even-mode SLR, which is then coupled to the slots. This symmetric design is devised to improve the polarization purity of the antenna.

Fig. 9 shows the comparison of the simulated S_{11} of the three patch antennas. As can be observed, Antenna-I has one reflection zero at 28 GHz and a bandwidth of 10% from 26.5 to 29.5 GHz. When the U-shaped slot is integrated in the ground, Antenna-II exhibits an improved bandwidth with two reflection zeros in the band. The FBW is about 17.8%. For the proposed antenna, the bandwidth is further enhanced to 24.9 to 31.6 GHz (FBW=24%). Compared with Antenna-I and II, the proposed antenna also shows a rapid roll-off at the both edges of the band. The improved selectivity can effectively reduce the channel interferences. Moreover, the removal of the cascaded mm-wave filter and the interfaces (ports) between them will significantly reduce the cost of the mm-wave systems.

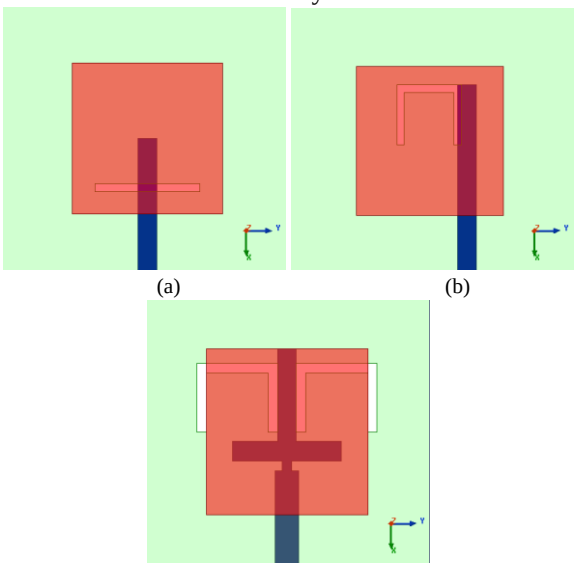

Fig. 8. Configuration of the three types of patch antennas: (a) traditional slot coupled patch antenna, Antenna-I, (b) U-shaped slot coupled patch antenna, Antenna-II, (c) proposed antenna.

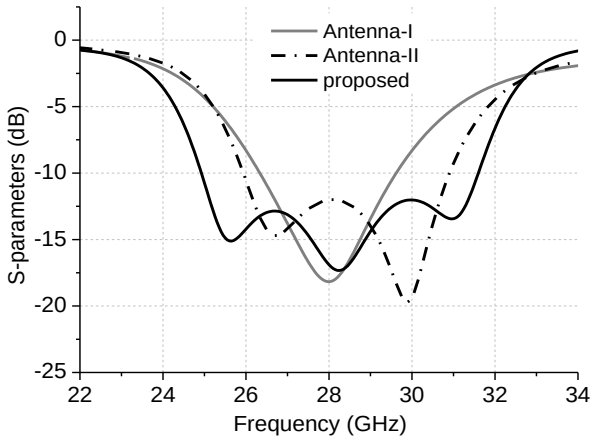

Fig. 9. Simulated S_{11} comparison of the three antennas presented in Fig. 8.

IV. Massive MIMO Antenna Array

Build on from the 4 × 4 subarray in Fig. 1, a planar massive MIMO antenna array for 5G base-station system is conceived, as shown in Fig. 10. It consists of four subarrays, indicated as 1, 2, 3 and 4. All of the subarrays have the same polarization in the X-axis direction. Each subarray consists of 4 × 4 radiation elements and thus high antenna gain can be achieved. Because of the planar structure, the whole MIMO antenna array has a very compact volume of 60 mm × 60 mm ×1.5 mm. Switchable radiation patterns are implemented in this design by adding different phase to the radiation elements. The beam of the subarray-1 is steered to –X direction, while the subarray-2 is steered to +X direction. The other two subarrays have their beams in the broadside direction. Fig. 11 shows the radiation patterns of the massive MIMO antenna when P1, P2 and P3 are

excited, respectively. As can be observed, subarray-1 and 2 have maximum radiations in φ = ± 26 degrees while subarray-3 radiates in φ= 0 degree.

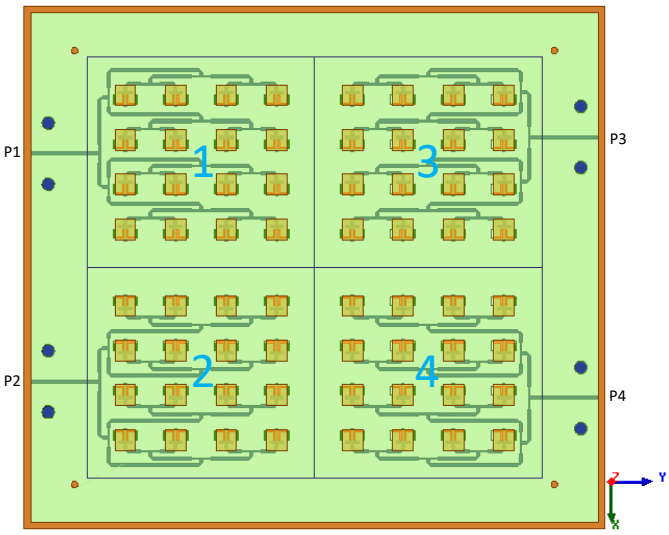

Fig. 10. Configuration of the proposed 2 × 2 messive MIMO antenna array for base station system.

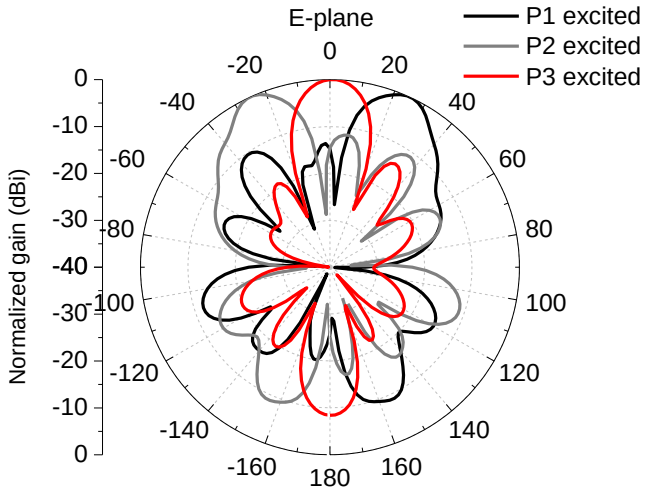

Fig. 11. The E-plane radiation patterns of the massive MIMO array antenna when P1, P2 and P3 are excited separately.

Fig. 12 presents the simulated current distribution at 28 GHz when different input ports are excited. When P1 is excited, as shown in Fig. 12(a), strong currents are distributed on the subarray-1. Because the antenna has the linear polarization in X-axis, the strongest mutual coupling occurs between the adjacent subarray-1 and subarray-2, which is revealed from the current distribution. The currents on the subarray-3 and 4 are very weak, and therefore the isolation between them is high.

The simulated mutual couplings between the four ports are shown in Fig. 13. As can be observed, the mutual coupling between P1 and P2 is stronger (with S_{21} at about -26 dB in band) than that between P1 and P3 (P4) which is below to -40 dB.

For base station applications, it is of interest to investigate the radiation characteristics of the MIMO array when two or more inputs are excited simultaneously. Here, the two subarrays (subarray-1 and 2) with the strongest mutual coupling are studied. Fig. 12(b) shows the current distribution when the P1 and P2 are excited simultaneously. It is shown

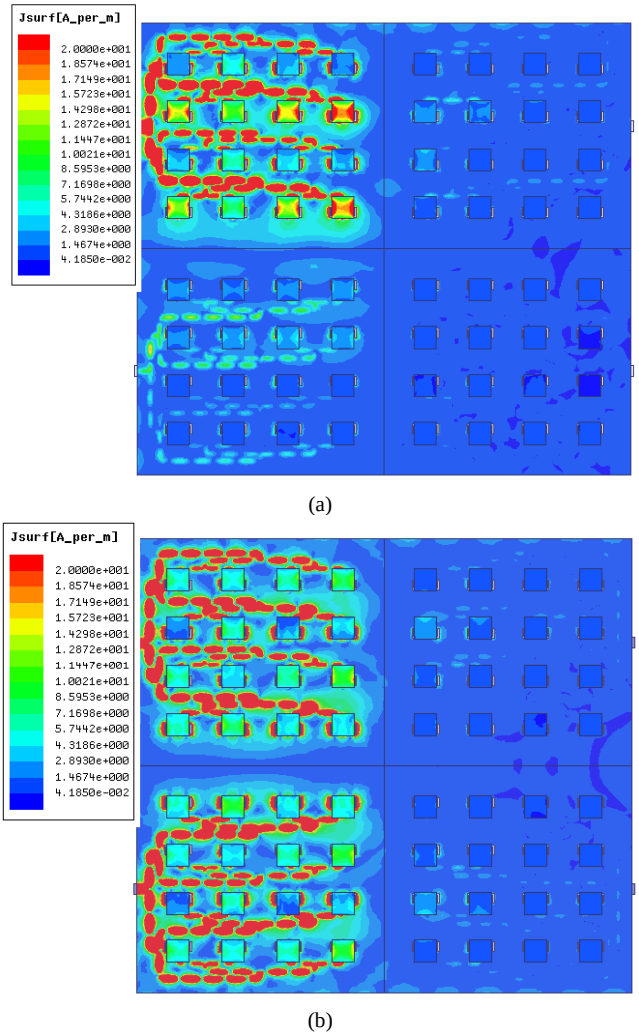

Fig. 12. The simulated current distribution of the massive MIMO array at 28 GHz: (a) P1 is excited, (b) P1 and P2 are excited.

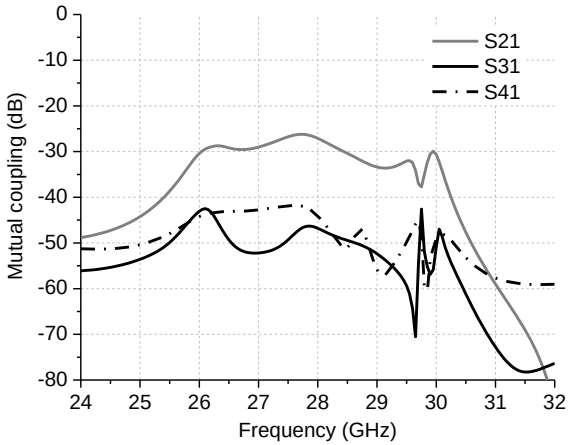

Fig. 13. Simulated mutual couplings between the four input ports of the massive MIMO array.

that the currents from each subarray are largely confined without much interference between each other. The currents coupled to the subarray-3 and 4 are very weak.

Fig. 14 shows the simulated 3-D and 2-D radiation patterns at 28 GHz when P1 and P2 are excited simultaneously. Two

main beams are shown in the E plane (XoZ) and the gain for

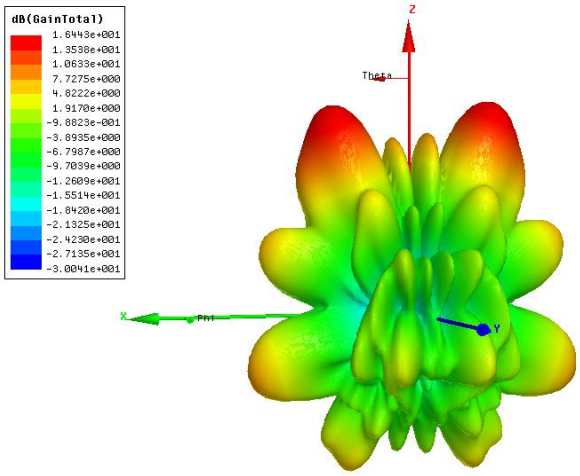

(a)

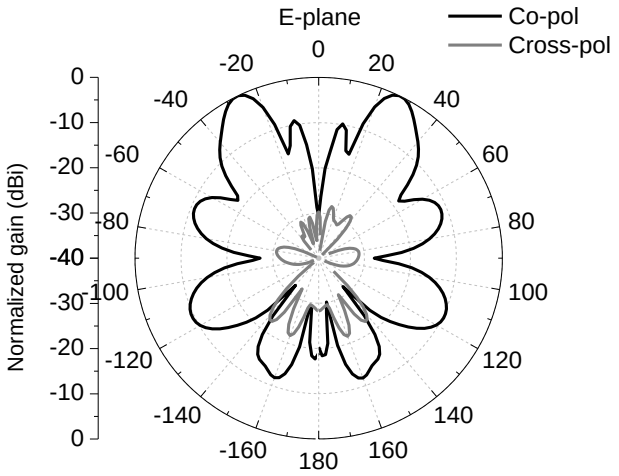

(b)

Fig. 14. The simulated radiation pattern at 28 GHz when P1 and P2 are excited: (a) 3-D pattern, (b) 2-D pattern in E-plane (XoZ plane).

each beam is about 16.4 dBi, as shown in Fig. 14(a). Fig. 14(b) shows the corresponding 2-D radiation pattern in the E-plane. The two main beams offset the broadside by 26.5 degrees. The MIMO antenna also exhibits a very good polarization performance with the cross polarization discrimination (XPD) in the main beams higher than 30 dB.

V. Results and Discussion

A. Broadband filtering subarray

The proposed 4 × 4 broadband filtering subarray is fabricated and the prototype is shown in Fig. 15. Fig. 16 presents the simulated and measured S_{11} of the subarray. It is observed that the measured result agrees reasonably well with the simulation, showing a very wide impedance bandwidth from 25.2 to 31 GHz (FBW = 21.6%). The broadband performance is attributed to the integrated design of the resonators and patch as well as the vertically coupled structures. The discrepancy between the simulation and the measurement is caused by the fabrication errors.

Fig. 17 shows the simulated and measured E-plane normalized radiation patterns of the 4 × 4 subarray at 26, 28

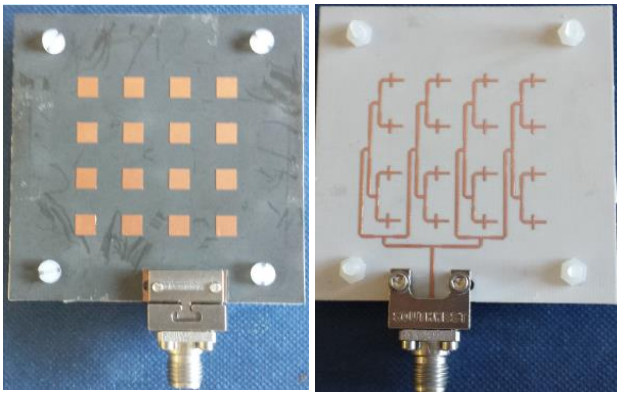

(a) (b)

Fig. 15. The prototype of the proposed subarray: (a) front-view, (b) back-view.

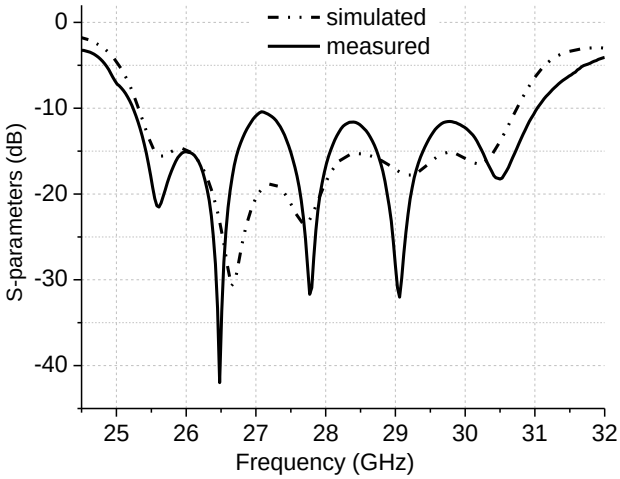

Fig. 16. Simulated and measured S_{11} of the proposed subarray.

and 30 GHz, respectively. As can be seen, the subarray has a broadside radiation patterns over a broadband. The measured results agree very well with the simulations, showing consistent radiation patterns and high XPD over the whole band. The measured side-lobe is below -12 dB and the XPD in the broadside is higher than 28 dB for all three frequency points. Fig. 18 shows the H-plane radiation patterns of the subarray, which show similar patterns as in the E-plane.

Fig. 19 shows the simulated and measured antenna gain of the subarray from 23 to 33 GHz. The simulated gain of a traditional patch antenna is also presented for comparison. It is observed that the measured results agree reasonably well with the simulated ones, showing a flat and high gain of 18 dBi from 6 to 30.5 GHz. Out of the band, the gain rapidly drops to below 10 dBi when the frequency is below 23.8 GHz and over 33 GHz. Compared with the traditional patch with the same stack structure, the proposed antenna demonstrates a good filtering characteristic.

B. Massive MIMO array

The 2 × 2 massive MIMO antenna array is fabricated and the prototype is shown in Fig. 20. The antenna is composed of 4 subarrays and 8 × 8 patches in total. On the bottom layer, there are four groups of feed networks. Fig. 21 shows the simulated

and measured mutual coupling between the four subarrays (inputs). Both the simulated and measured results

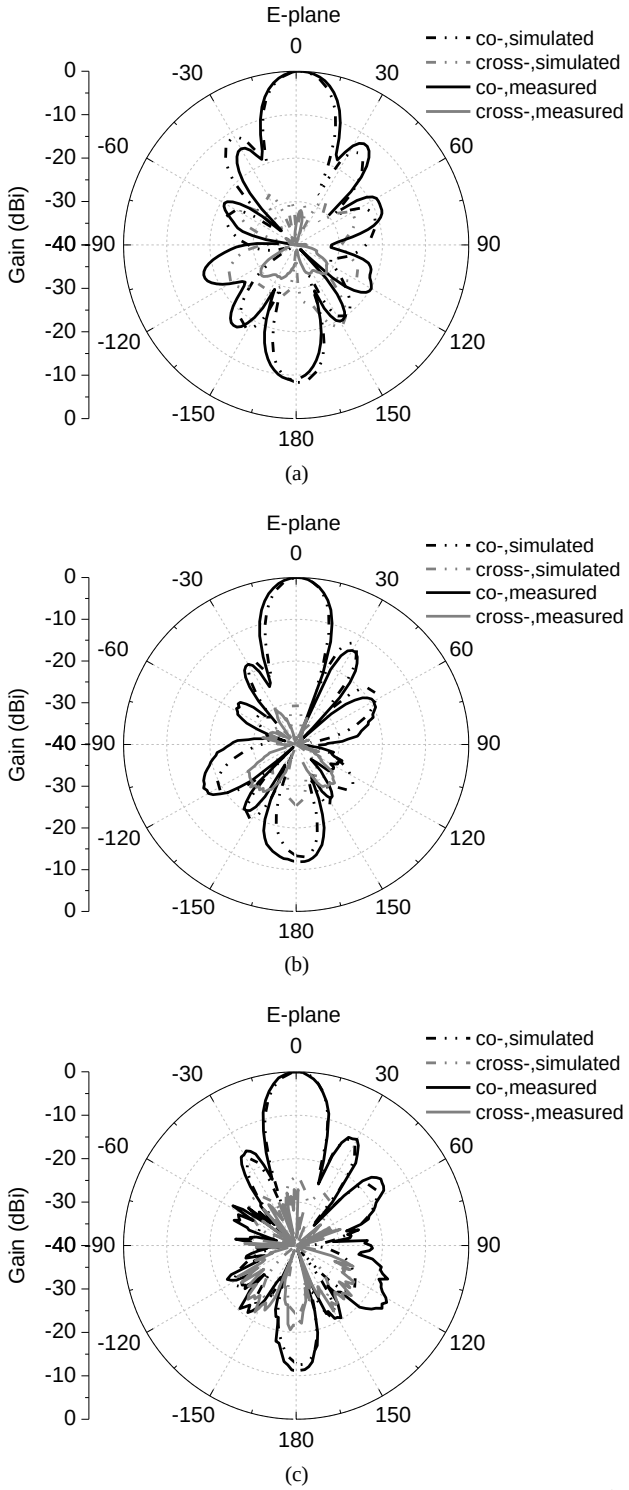

Fig. 17. Simulated and measured normalized E-plane radiation patterns of the subarray: (a) 26 GHz, (b) 28 GHz and (c) 30 GHz.

show the MIMO antenna has high isolation between the subarrays. The most significant mutual coupling occurs between the subarray 1 and 2 and the measured $|S_{21}|$ is about -28 dB. The isolation between the subarray 1 and 3 (4) are higher than 37 dB.

Fig. 22 shows the simulated and measured normalized radiation patterns of the massive MIMO antenna in E-plane. When the P1 is excited and the other ports are terminated with

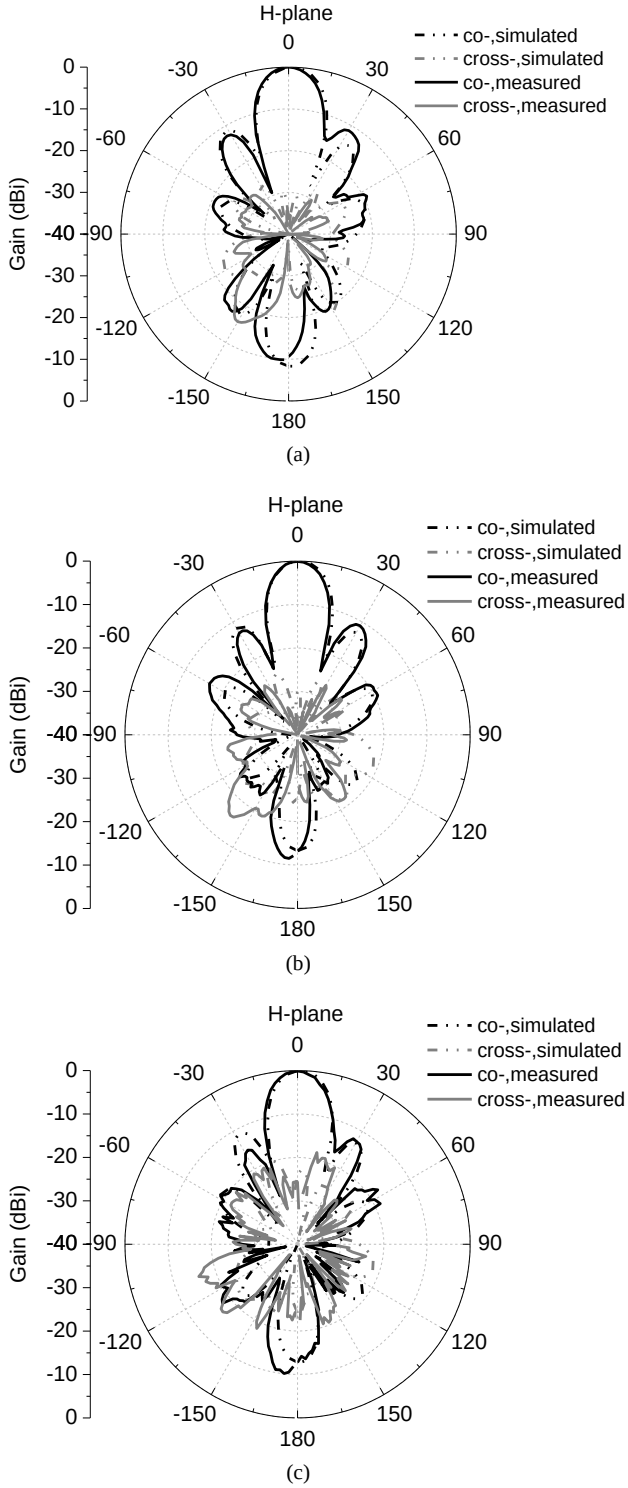

Fig. 18. Simulated and measured normalized H-plane radiation patterns of the subarray: (a) 26 GHz, (b) 28 GHz and (c) 30 GHz.

a 50 Ω load, the main beam is steered to an angle of 26 degrees.

The side-lobes are lower than the main beam by more than 10 dB. The antenna shows a very good polarization performance in the main beam with the XPD lower than -30 dB. The peak gain is 16.3 dBi for the measurement. When P2 is

excited, the antenna exhibits a similar radiation pattern in the E-plane but the main beam is steered to -26 degrees. The

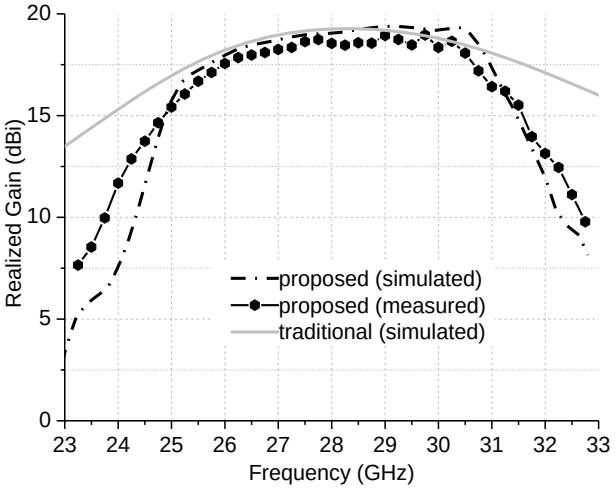

Fig. 19. Simulated and measured antenna gains of the proposed subarray.

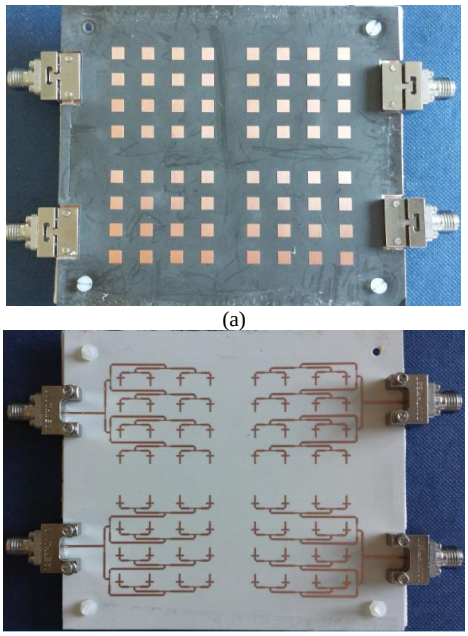

(a)

(b)

Fig. 20. The prototype of the 2 × 2 massive MIMO antenna array: (a) front-view, (b) back-view.

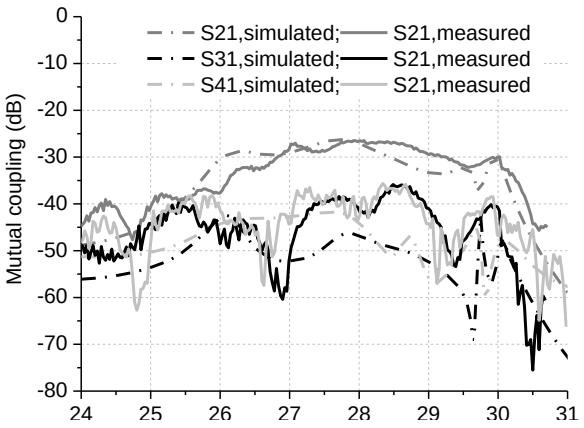

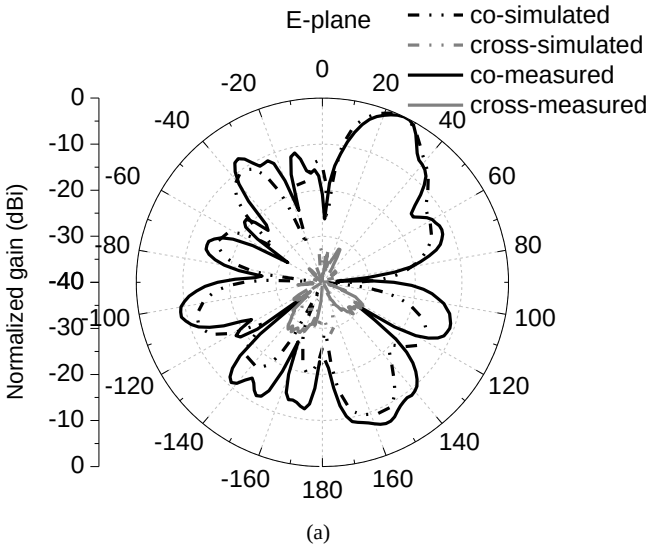

(a)

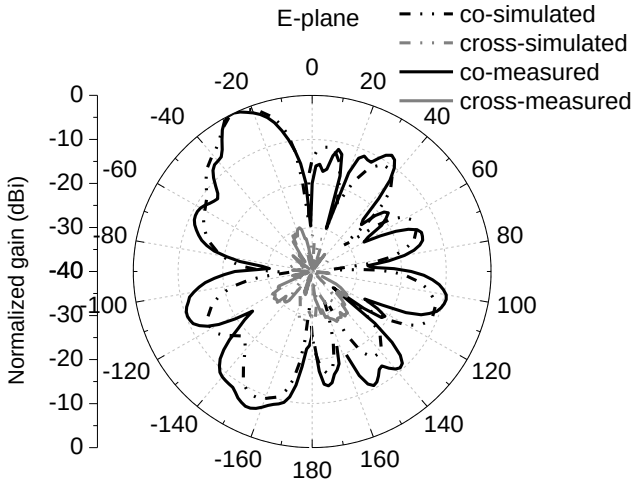

(b)

Fig. 22. The simulated and measured normalized radiation patterns at 28 GHz: (a) P1 is excited, (b) P2 is excited.

peak gain is 16.6 dBi for the measurement. The measured and simulated radiation patterns agree well with each other. Fig. 17 and 18 broadly represent the radiation patterns of the subarray 3 and 4 thus they are not shown here.

VI. Conclusion

In this paper, a broadband planar millimeter-wave (28 GHz) massive MIMO antenna array is proposed for 5G base station applications. The MIMO antenna is composed of 2 × 2 subarrays and each subarray consists of 4 × 4 patch antennas with a 3rd-order filtering characteristic. The integrated filtering antenna is achieved by vertically coupling together the patch radiator, the slot resonators in the ground plane and the SLR attached to the feed line. A broad bandwidth of 25% is achieved by virtue of the strong couplings. The design methodology and processes are detailed. The performances of the MIMO antenna array, such as impedance matching, mutual coupling and radiation patterns, are investigated. In addition, beam switching capability is also demonstrated and a steering angle of ±26 degrees can be achieved. Such switchable patterns with high

gain at the base station can be used to service users at different locations or users in motion. The subarray and the MIMO array antenna are prototyped and tested, showing a broad bandwidth, high gain, and good out-of-band rejection. The integration of filter-antenna removes the need of separate cascaded millimeter filters and the 50 Ω interfaces. As a result, the cost of the mm-wave front-end system can be reduced. Such features and advantages are very useful for 5G base station applications.

REFERENCES

[1] T. Rappaport, S. Sun, R. Mayzus, H. Zhao, Y. Azar, K. Wang, G. Wong, J. Schulz, M. Samimi and F. Gutierrez, "Millimeter wave mobile communications for 5G cellular: It will work!," *IEEE Access*, vol. 1, pp. 335-349, 2013.

[2] Samsung. (2015, Aug.). Samsung demo: 5G vision, Korea. Available: http://www.samsung.com/global/business/networks/insights/news/samsung-electronics-sets-5g-speed-record-at-7-5gbpsover-30-times-faster-than-4g-lte.

[3] F. Rusek, D. Persson, B. Lau, E. Larsson, T. Marzetta, O. Edfors and F. Tufvesson, ``Scaling up MIMO: Opportunities and challenges with very large arrays," *IEEE Signal Process. Mag.*, vol. 30, no. 1, pp. 40-60, Jan. 2013.

[4] F. Rusek, D. Persson, B. K. Lau, E. G. Larsson, T. L. Marzetta, O. Edfors, and F. Tufvesson, "Scaling up mimo: Opportunities and challenges with very large arrays," *IEEE Signal Process. Mag*., vol. 30, no. 1, pp. 40–60, Jan. 2013.

[5] E. Larsson, O. Edfors, F. Tufvesson, and T. Marzetta, "Massive mimo for next generation wireless systems," *IEEE Commun. Mag*., vol. 52, no. 2, pp. 186–195, Feb. 2014.

[6] S. Ershadi, A. Keshtkar, A. Abdelrahman, X. Yu and H. Xin, "Design of wideband unit-cell element for 5G antenna arrays," *2015 Asia-Pacific Microwave Conference (APMC)*, pp. 1-3, 2015.

[7] J. S. Park, J. B. Ko, H. K. Kwon, B. S. Kang, B. Park and D. Kim, "A tilted combined beam antenna for 5G communications using a 28-GHz Band," *IEEE Antennas Wireless Propog*. *Lett*, vol. 15, pp. 1685-1688, 2016.

[8] H. Aliakbari, A. Abdipour, R. Mirzavand, A. Costanzo and P. Mousavi, "A single feed dual-band circularly polarized millimeter-wave antenna for 5G communication," *2016 10th European Conference on Antennas and Propag. (EuCAP)*, pp. 1-5, 2016.

[9] W. Hong, K. H. Baek, Y. Lee, Y. Kim and S. T. Ko, "Study and prototyping of practically large-scale mmWave antenna systems for 5G cellular devices," *IEEE Communications Magzine*, vol. 52, no. 9, pp. 63-69, 2014.

[10] W. Zhai, V. Miraftab, M. Repeta, D. Wessel and W. Tong, "Dual-band millimeter-wave interleaved antenna array exploiting low-cost PCB technology for high speed 5G communication," *2016 IEEE MTT-S International Microw. Symposium (IMS)*, pp. 1-4, 2016.

[11] F. F. Manzillo, M. Ettorre, M. Lahti, K. Kautio, D. Lelaidier, E. Seguenot, R. Sauleau, "A multilayer LTCC solution for integrating 5G access point antenna modules," *IEEE Trans. Microw. Theory Techn*., vol. 64, no. 7, pp. 2272-2283, 2016.

[12] J. Hirokawa, "Millimeter-wave antenna technologies for 5G mobile communication systems," *2016 IEEE International Workshop on Electromagnetics: Applications and Student Innovation Competition (iWEM)*, pp. 1-3, 2016.

[13] M. M. Ali, A. R. Sebak, "Design of compact millimeter wave massive MIMO dual-band (28/38 GHz) antenna array for future 5G communication systems," *2016 17th International Symposium on Antenna Technology and Applied Electromagnetics (ANTEM)*, pp. 1-2, 2016.

[14] Y. Gao, R. Ma, Y. Wang, Q. Zhang and C. Parini, "Stacked patch antenna with dual-polarization and low mutual coupling for massive MIMO," *IEEE Trans. Antennas and Propag.*, to be published.

[15] C. X. Mao, S. Gao, Y. Wang, F. Qin and Q. X. Chu, "Multi-mode resonator-fed dual polarized antenna array with enhanced bandwidth and selectivity," *IEEE Trans. Antennas and Propag.*, vol. 63, no. 12, pp. 5492–5499, Dec. 2015.

[16] X. Y. Zhang, W. Duan, Y. M. Pan, "High-gain filtering patch antenna without extra circuit," *IEEE Trans. Antennas Propag.*, vol. 63, no. 12, pp. 5883-5888, Dec. 2015.

[17] C. X. Mao, S. Gao, Y. Wang, Z. Wang, F. Qin, B. Sanz, Q. X. Chu, "An integrated filtering antenna array with high selectivity and harmonics suppression," *IEEE Trans. Microw. Theory Techn*., vol. 64, no. 6, pp. 1798-1805, Apr. 2016.